arXiv:1410.3372v2 [quant-ph] 9 Dec 2014

Entanglement of neutral-atom chains by spin-exchange Rydberg interaction

Xiao-Feng Shi,[1] F. Bariani,[2] and T. A. B. Kennedy[1]

[1]*School of Physics, Georgia Institute of Technology, Atlanta, GA, 30332-0430, USA*
[2]*Department of Physics, College of Optical Sciences and B2 Institute, University of Arizona, Tucson, Arizona 85721, USA*

(Dated: December 10, 2014)

Conditions to achieve an unusually strong Rydberg spin-exchange interaction are investigated and proposed as a means to generate pairwise entanglement and realize a SWAP-like quantum gate for neutral atoms. Ground-state entanglement is created by mapping entangled Rydberg states to ground states using optical techniques. A protocol involving SWAP gate and pairwise entanglement operations is predicted to create global entanglement of a chain of N atoms in a time that is independent of N.

PACS numbers: 03.67.Bg, 03.65.Ud, 32.80.Ee, 32.80.Xx

I. INTRODUCTION

Entanglement is a property of multiparticle quantum states that is essential for implementing quantum information or computation protocols [1, 2]. As a result, schemes for the fast and efficient generation of entanglement among many quantum systems are the subject of intense theoretical and experimental efforts. Atoms offer an ideal arena for the demonstration of quantum protocols given the stability of their ground states and the powerful optical and trapping techniques that have been developed to control their internal and external degrees of freedom [3]. The excitation of Alkali atoms to energy levels of large principal quantum number, generically named Rydberg states, provides a way to enhance by several orders of magnitude otherwise weak neutral atom interactions. The resulting dipole-dipole or van der Waals interaction between two highly excited Rydberg atoms allows the creation of stable entangled states of atoms in their ground electronic level [4–12]. The methods employed to date [4–9] rely on the Rydberg blockade effect, in which two-atom energy levels with two Rydberg excitations experience a large interaction induced shift, while energy levels with a single Rydberg excitation are unperturbed. As a consequence, under conditions in which a single Rydberg excitation is resonantly excited, the pair excitation probability is strongly suppressed [13–20].

The excitation of two atoms into Rydberg S-orbitals with different principal quantum numbers, $n_{\rm A}$ and $n_{\rm B}$, and opposite electron spin orientation, produces not only the Rydberg blockade shift [21–28], but also a coupling that exchanges the electron spin states. While the blockade shift is usually the dominant effect, the spin-exchange coupling can be made almost equally strong with the right choice of $n_{\rm A}$ and $n_{\rm B}$. In this regime, when nearby atoms are optically driven, the probability to create double Rydberg excitations can be as large as one, in sharp contrast to the case when $n_{\rm A} = n_{\rm B}$. Furthermore, the two-atom Rydberg state created by this mechanism is one of two entangled Bell states, the triplet denoted $|r_+\rangle$, in the subspace of the two-atom Rydberg excitations. The orthogonal Rydberg Bell state, the singlet $|r_-\rangle$, experiences a strong level shift and is effectively decoupled from the excitation. The entangled Rydberg state created in this way is metastable, but the entanglement can be mapped optically to the ground state in a time short compared to the metastable state lifetime. In the following, we explain how to produce ground state entanglement of a pair of atoms by a sequence of three pulses, and then discuss a protocol for global entanglement of a chain of atoms involving a sequence of twelve pulses which minimizes the blockade shifts due to multiple Rydberg excitations along the chain.

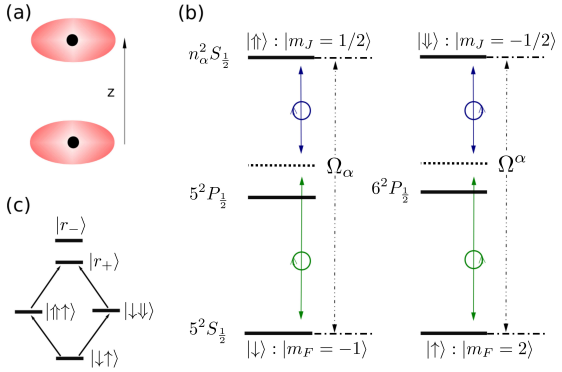

FIG. 1: (Color online) Schematic illustration for generating entanglement between two ^{87}Rb atoms. (a) Geometry considered with atoms (black dots) in tightly focused optical traps (shaded regions) along the quantization axis **z**. (b) Laser excitation of atom $\alpha = A, B$ by two-photon transitions. The two-photon transition via the 5P (6P) state of atom α has an effective Rabi frequency Ω_α(Ω^α). (c) Relevant levels in the excitation of Rydberg Bell state $|r_+\rangle$.

The main body of the paper gives an account of the novel interaction mechanism and its applications to quantum computation. Section II introduces the spin-exchange interaction and its potential for two-atom entanglement. Section III discusses an example to achieve pairwise entanglement via optical pumping. In Sec. IV,

we investigate the pairwise entanglement efficiency by numerical simulation. In Sec. V, we study a quantum gate that is similar to the SWAP gate, and introduce a protocol of global entanglement of atoms in a chain. Section VI gives a summary. Additional details of the theory are given in the appendices.

II. TWO-ATOM ENTANGLEMENT

Consider two ^{87}Rb atoms, denoted A and B, respectively, which are loaded into two far-off-resonant traps created by tightly focused laser beams. The interatomic axis is defined by the vector $\mathbf{z}$. Each of the atoms can be independently driven by laser light, as shown in Fig. 1. We suppose atom A is prepared in a hyperfine level of the ground state manifold identified as "spin-up" while atom B is prepared in the state "spin-down": $|\uparrow\rangle_{\rm A}(|\downarrow\rangle_{\rm B}) \equiv |5^2S_{\frac{1}{2}}, F=2, m_F=2(-1)\rangle$. These states may be optically coupled via two-photon transitions to the Rydberg states $|\Downarrow\rangle_{\rm A}(|\Uparrow\rangle_{\rm B}) \equiv |n_{\rm A(B)}\ ^2S_{\frac{1}{2}}, m_J=\mp 1/2\rangle$ of atoms A and B, respectively. Here we use the hyperfine notation to label ground states and the fine structure notation for Rydberg levels, according to the spectroscopic resolution usually achieved in experiments (see Appendix A).

Consider two Rydberg atoms prepared in the states $|\Uparrow\rangle_{\rm A}$ and $|\Downarrow\rangle_{\rm B}$, respectively, and separated by a distance L large enough that the states are coupled by the C_6/L^6 van der Waals interaction [7, 29]. In the case $n_{\rm A}=n_{\rm B}$, this coupling is dominant and induces a shift of the doubly excited Rydberg state commonly referred to as the blockade shift. When $n_{\rm A}\neq n_{\rm B}$, and under special conditions, the coupling $C_6^{\rm ex}/L^6$, which exchanges the electronic spin states, may become equally large. In the two-atom product basis $|\Uparrow\Downarrow\rangle$, $|\Downarrow\Uparrow\rangle$, the total van der Waals interaction is then,

$$H_{\rm v} = \frac{1}{L^6}\begin{pmatrix} C_6 & C_6^{\rm ex} \\ C_6^{\rm ex} & C_6 \end{pmatrix}. \qquad (1)$$

By using the measured results for the relevant quantum defects [30] and a semiclassical expression for the radial matrix elements [31], we numerically evaluate C_6 and $C_6^{\rm ex}$ for $0 \le n_{\rm B}-n_{\rm A} \le 10$ and $50 < n_{\rm B} < 129$. We find four pairs of states where the interaction coefficients differ by less than 2%; see Table I.

The occurrence of a strong spin-exchange interaction in these cases arises through an interference effect involving a small number of dominant intermediate $p_{1/2}$ and $p_{3/2}$ states (see Appendix B). We find that the transition matrix elements for spin exchange constructively interfere whereas a partially destructive interference limits the blockade shift. This results in almost equal magnitude of C_6 and $C_6^{\rm ex}$.

The eigenstates and eigenvalues of Eq. (1) are $|r_\pm\rangle \equiv (|\Uparrow\Downarrow\rangle \pm |\Downarrow\Uparrow\rangle)/\sqrt{2}$, and $V_\pm \equiv (C_6 \pm C_6^{\rm ex})/L^6$. If the interaction coefficients have equal magnitudes, one of the two energy eigenvalues is unshifted from the non-interacting value. For the four cases shown in Table I, C_6 and $C_6^{\rm ex}$ have opposite signs, and by choosing an appropriate atomic separation L, V_- (V_+) can be made much larger (smaller) than the excitation Rabi frequency. As a result, atoms A and B will be excited to the entangled two-atom Rydberg state $|r_+\rangle$. The lifetime of the entanglement created can be enhanced by coupling it to the two-atom ground state, by driving Rabi oscillations $|\downarrow\rangle \leftrightarrow |\Uparrow\rangle$ and $|\uparrow\rangle \leftrightarrow |\Downarrow\rangle$ simultaneously on both atoms [Fig. 1(b)], so that the Rydberg triplet state $|r_+\rangle$ is mapped to the ground level Bell state

$$|g_+\rangle \equiv (|\uparrow\downarrow\rangle + |\downarrow\uparrow\rangle)/\sqrt{2}. \qquad (2)$$

$n_{\rm A}$	$n_{\rm B}$	$C_6/(2\pi)$	$C_6^{\rm ex}/(2\pi)$
59	61	-196	194
73	75	4080	-4025
97	100	-59780	58800
121	124	1104000	-1124000

TABLE I: Strength of blockade and spin-exchange interactions between two atoms of principle quantum numbers $n_{\rm A}$ and $n_{\rm B}$. $C_6, C_6^{\rm ex}$ are in unit of GHz μm^6.

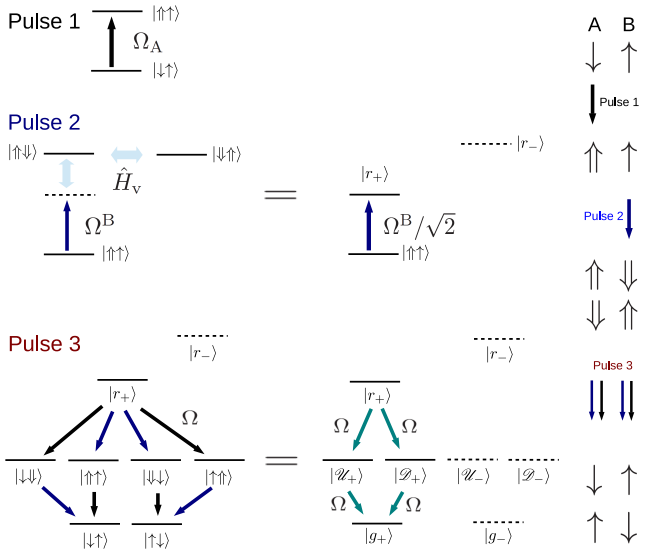

FIG. 2: (Color online) Schematic of the entanglement protocol via pulses 1, 2 and 3. During pulse 1 (2), only the two-photon transition via 5P (6P) state of atom A (B) is excited with Rabi frequency Ω_A (Ω^B). During pulse 3, the four two-photon transitions via 5P and 6P states of atoms A and B are turned on and the magnitudes of these two-photon Rabi frequencies are set equal to Ω. On the left column we show the bare two-atom basis, while on the right we highlight the superposition states involved.

III. PAIRWISE ENTANGLEMENT PROTOCOL

We now describe the complete protocol creating ground state entanglement via a three-π-pulse sequence.

Pulse 1 on atom A: We take the initial state to be $|{\downarrow}{\uparrow}\rangle$. The first pulse acts on atom A and excites $|{\downarrow}\rangle$ to $|{\Uparrow}\rangle$ via the $5P$ state, as shown in Fig. 2. Since atom B is in its ground state, there is no Rydberg interaction. Thus, by applying a pulse of duration $\tau_1 = \pi/\Omega_{\rm A}$, we generate the product state $|{\Uparrow}{\uparrow}\rangle$.

Pulse 2 on atom B: Following pulse 1, apply a two-photon laser pulse to atom B with Rabi frequency $\Omega^{\rm B}$, as shown in Fig. 2. This pulse excites $|{\uparrow}\rangle$ to $|{\Downarrow}\rangle$ via the $6P$ state as in Fig. 1(b). The evolution of the two-atom wave function $|\Psi\rangle$ is governed by the Hamiltonian

$$H_{\rm Pulse2} = \frac{1}{2\sqrt{2}} \begin{pmatrix} 0 & \Omega^{\rm B} & \Omega^{\rm B} \\ \Omega^{\rm B} & 2\sqrt{2}V_+ & 0 \\ \Omega^{\rm B} & 0 & 2\sqrt{2}V_- \end{pmatrix}, \qquad (3)$$

where the basis vectors are $|{\Uparrow}{\uparrow}\rangle$,$|r_+\rangle$ and $|r_-\rangle$. In the case of $|V_-| \gg \Omega^{\rm B}$, we can adiabatically eliminate the state $|r_-\rangle$. The population on the Rydberg Bell state $|r_+\rangle$ reaches its maximum

$$|\langle r_+|\Psi\rangle| \approx 1 - (V_+/\Omega^{\rm B})^2, \qquad (4)$$

for a pulse of duration $\tau_2 = (\sqrt{2}\pi/\Omega^{\rm B})\left[1-(V_+/\Omega^{\rm B})^2\right]$. The prefactor $\sqrt{2}\pi/\Omega^{\rm B}$, indicates that this is a two-atom π-pulse, while the correction $V_+^2/(\Omega^{\rm B})^2$ results from the small shift of $|r_+\rangle$.

Pulse 3 on both atoms: The final step is the mapping of the entangled state of Rydberg atoms onto the ground states. In contrast to Pulses 1 and 2, switch on all four Rabi channels simultaneously exciting the two atoms, as shown in Fig. 1(b).

When the Rabi frequencies satisfy $\Omega \equiv \Omega_{\rm A} = \Omega^{\rm A} = \Omega_{\rm B} = \Omega^{\rm B}$, only the intermediate states $|\mathscr{U}_+\rangle$ and $|\mathscr{D}_+\rangle$ are coupled to $|r_+\rangle$ and $|g_+\rangle$, where $|\mathscr{U}_\pm\rangle \equiv [|{\Uparrow}{\uparrow}\rangle \pm |{\uparrow}{\Uparrow}\rangle]/\sqrt{2}$ and $|\mathscr{D}_\pm\rangle \equiv [|{\Downarrow}{\downarrow}\rangle \pm |{\downarrow}{\Downarrow}\rangle]/\sqrt{2}$, see Fig. 2. Ordering the states $|r_+\rangle$, $|\mathscr{U}_+\rangle$, $|\mathscr{D}_+\rangle$ and $|g_+\rangle$ the Hamiltonian matrix during Pulse 3 reads,

$$H_{\rm Pulse3} = \frac{1}{2} \begin{pmatrix} 2V_+ & \Omega & \Omega & 0 \\ \Omega & 0 & 0 & \Omega \\ \Omega & 0 & 0 & \Omega \\ 0 & \Omega & \Omega & 0 \end{pmatrix}. \qquad (5)$$

At the end of Pulse 3, of duration π/Ω, the entangled Rydberg state $|r_+\rangle$ would be completely mapped onto the entangled ground state $|g_+\rangle$ with fidelity limited by the residual shift V_+, and the radiative decay rate of the Rydberg level.

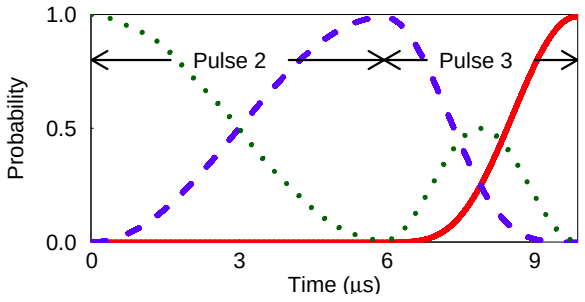

FIG. 3: (Color online) Evolution of the two-atom state during pulses 2 and 3 of the entanglement protocol, starting from $|{\Uparrow}{\uparrow}\rangle$. We plot the populations of the relevant states from the basis in Eq. (7): the red (gray) solid line is $|\mathcal{G}_+|^2$, the blue (dark gray) dashed line is $|\mathcal{R}_+|^2$, the green (light gray) dotted line is $\sum_\eta[|\mathcal{U}_\eta|^2 + |\mathcal{D}_\eta|^2]$.

IV. NUMERICAL SIMULATION AND FIDELITY

The proposed scheme relies on creation of the Rydberg entangled state, $|r_+\rangle$, which requires

$$|V_-| \gg \Omega \gg |V_+|. \qquad (6)$$

In order to show that the ground Bell state $|g_+\rangle$ can be prepared with high fidelity for finite $|V_-/V_+|$, we numerically study the time evolution of the atomic state following the procedure discussed above. We choose the Rydberg state pair with principal quantum numbers $n_{\rm A} = 73$, $n_{\rm B} = 75$, atomic separation $L = 15\mu$m, and set the single-atom Rabi frequency $\Omega = \Omega^{\rm B} = \sqrt{|V_-V_+|} = 2\pi \times 59$ kHz. We expand the two-atom wavefunction as

$$|\Psi\rangle = \sum_{\eta=\pm} \left[\mathcal{G}_\eta|g_\eta\rangle + \mathcal{R}_\eta|r_\eta\rangle + \mathcal{U}_\eta|\mathscr{U}_\eta\rangle + \mathcal{D}_\eta|\mathscr{D}_\eta\rangle\right], \qquad (7)$$

and we numerically solve the Schrödinger equation for Pulses 2 and 3 (see Appendices C and D), since pulse 1 is trivial. The achieved ground state fidelity is $\mathcal{F} = |\langle g_+|\Psi\rangle|^2 = 98.5\%$. To improve the fidelity of the prepared ground Bell state, we numerically optimize $\mathcal{F}$ by varying Rabi frequencies and pulse durations. Figure 3 shows the state evolution with $\Omega^{\rm B}/(2\pi) = 119$ kHz and $\Omega/(2\pi) = 128$ kHz: a fidelity of $\mathcal{F}_1 = 99.06\%$ for the ground Bell state $|g_+\rangle$ is achieved in less than ten microseconds.

The main practical difficulty is to have all four Rabi frequencies for the excitation channels equal to each other. In order to show that the the protocol is robust against dispersion in the Rabi frequencies, we numerically integrate the Schrödinger equation varying $\Omega_{\rm A}, \Omega^{\rm A}, \Omega_{\rm B}$ and $\Omega^{\rm B}$ in the interval $[1-\epsilon,\ 1+\epsilon]\Omega$ for Pulse 3, with $\Omega = \sqrt{V_+V_-}$, $\tau_2 = (\sqrt{2}\pi/\Omega)\left[1-(V_+/\Omega)^2\right]$, and $\tau_3 = \pi/\Omega$. By performing 10^5 such simulations, we find that almost all fidelities are larger than 95% (85%) for $\epsilon = 0.1$ (0.2) (see Appendix D).

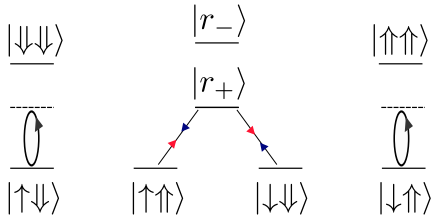

FIG. 4: (Color online) Schematic of the SWAP-like gate protocol. During the 2π pulse, $|r_-\rangle$, $|\Downarrow\Downarrow\rangle$ and $|\Uparrow\Uparrow\rangle$ are hardly excited due to Rydberg blockade, while $|r_+\rangle$ will be excited, forming a Λ system with $|\downarrow\Downarrow\rangle$ and $|\uparrow\Uparrow\rangle$.

V. SWAP GATE AND ENTANGLEMENT OF ATOMIC CHAINS

The spin-exchange Rydberg interaction may be used together with Rydberg blockade to implement a quantum logic gate based on a simple combination of three single-atom laser interaction processes: two π-pulses applied to atom B, are separated by an intermediate 2π-pulse applied to atom A. If both atoms are initially prepared in the same ground state, we obtain the state transformations,

$$|\uparrow\uparrow\rangle \xrightarrow[\text{atom B}]{\pi} |\uparrow\Downarrow\rangle \xrightarrow[\text{atom A}]{2\pi} |\uparrow\Downarrow\rangle \xrightarrow[\text{atom B}]{\pi} |\uparrow\uparrow\rangle,$$
$$|\downarrow\downarrow\rangle \xrightarrow[\text{atom B}]{\pi} |\downarrow\Uparrow\rangle \xrightarrow[\text{atom A}]{2\pi} |\downarrow\Uparrow\rangle \xrightarrow[\text{atom B}]{\pi} |\downarrow\downarrow\rangle.$$

During stages 1 and 3, a single Rydberg excitation is created and removed, while in stage 2, Rydberg blockade of the states $|\Downarrow\Downarrow\rangle$ and $|\Uparrow\Uparrow\rangle$, respectively, prevents any double excitation. Alternatively, when the atoms are initially prepared in opposite spin ground states, there is a crucial difference. As a consequence of the strong spin-exchange interaction, the 2π pulse resonantly couples to the triplet state $|r_+\rangle$ and flips the spin of both the Rydberg excitation and the atomic ground state; see Fig. 4. In this case the combination of van der Waals interaction and single atom 2π pulse creates a resonant "lambda" transition between two-atom states:

$$|\downarrow\uparrow\rangle \xrightarrow[\text{atom B}]{\pi} |\downarrow\Downarrow\rangle \xrightarrow[\text{atom A}]{2\pi(\Lambda)} -|\uparrow\Uparrow\rangle \xrightarrow[\text{atom B}]{\pi} -|\uparrow\downarrow\rangle,$$
$$|\uparrow\downarrow\rangle \xrightarrow[\text{atom B}]{\pi} |\uparrow\Uparrow\rangle \xrightarrow[\text{atom A}]{2\pi(\Lambda)} -|\downarrow\Downarrow\rangle \xrightarrow[\text{atom B}]{\pi} -|\downarrow\uparrow\rangle.$$

The three stage protocol completes the quantum SWAP gate transformation, with a π phase shift of the swapped states. By choosing $L = 15\mu$m and Rabi frequency 89kHz for the 2π pulse on atom A, we can demonstrate a gate fidelity $\mathcal{F}_{\rm SWAP} = 98.31\%$ for an operation time $\tau_{\rm SWAP} = 11\mu$s.

The combination of quantum SWAP gate with pairwise atom entanglement operations can be used as the basis of a protocol to entangle a chain of an arbitrary number of atoms. The key observation is that the atoms should be entangled sequentially in pairs, allowing gaps between the pairs in order to minimize spurious level shifts due to Rydberg blockade. After the pair-entanglement, a series of SWAP gate operations link all the pairs in a fully entangled state. Such a procedure may be easily sketched for the case of $4N$ atoms, where the atoms are labeled sequentially: A_1, B_1, C_1, D_1, $\cdots$, A_{4N}, B_{4N}, C_{4N}, D_{4N}. We first use the two-atom entanglement protocol described above to entangle atoms A_j and B_j, where $j = 1, \cdots, N$. This is followed by a similar protocol that entangles atoms C_j and D_j. Because all atoms are now entangled with one of their two neighboring atoms, the two-qubit SWAP gate is used to entangle atoms B_j and C_j, followed by another SWAP operation for entanglement of D_j and A_{j+1}. In this way we may entangle all $4N$ atoms by a twelve-pulse protocol as shown in Fig. 5. In the case of 4 atoms, this protocol generates the entangled state $(|\uparrow\downarrow\downarrow\uparrow\rangle + |\downarrow\uparrow\uparrow\downarrow\rangle - |\uparrow\uparrow\downarrow\downarrow\rangle - |\downarrow\downarrow\uparrow\uparrow\rangle)/2$, after the application of 9 pulses (see Appendix E).

During the pairwise entanglement and SWAP gate operations, the metastable Rydberg states are populated for a time τ, thus the fidelity of the entanglement of the $4N$-atom chain may be estimated as $\mathcal{F} \sim (\mathcal{F}_1 e^{-2\gamma\tau})^{2N} (\mathcal{F}_{\rm SWAP} e^{-2\gamma\tau})^{2N-1}$, where γ^{-1} is the lifetime of the Rydberg level. When keeping the leading order term after expanding the exponential of $\mathcal{F}$ under the condition of $\gamma\tau \ll 1$, the total error of the prepared many-atom entangled state scales linearly with N. Numerical simulations show that pairwise entanglement and SWAP gate operations can each be carried out in around 10μs. Thus a 4-atom chain may be entangled in a time $T = 30\mu$s with $L = 15\mu$m. For (a) $(n_A, n_B) = (73, 75)$, $\gamma^{-1} = 0.45$ ms for $n = 73$ and $\mathcal{F} \sim 90\%$, while for (b) $(n_A, n_B) = (97, 100)$, $\gamma^{-1} = 1$ ms for $n = 97$ and $\mathcal{F} \sim 94\%$ [7]. Decreasing L to $11.9\mu m$ makes $V_\pm$ four times larger, and reduces T to $7.5\mu s$. Then For $(n_A, n_B) = (73, 75)$, a 4-atom chain can be entangled with $\mathcal{F} \sim 95\%$, while an 8-atom chain can be entangled with $\mathcal{F} \sim 90\%$. These fidelities are comparable to the values for 4 and 8 atom entanglement by asymmetric blockade in Ref. [5] and dissipation in Ref. [11]. The dissipative protocol in [11] does not suffer from the spontaneous emission issue, but in comparison the present coherent process is almost three orders of magnitude faster. Furthermore, the linear scaling of the error with the total number of entangled atoms is similar to the the blockade-based situation of Ref. [5]: in that case the error scales cubically at low N and then saturates to a linear behavior. By contrast to the multi-atom entanglement based on Ryberg interactions and adiabatic passage proposed in Ref. [4], the duration and the Rabi frequency of our scheme are independent of N. The requirements on the Rabi frequencies and principal quantum numbers are well within experimental reach and the individual atomic addressing allows to tailor the distance between the atoms as well as the desired target state. All these considerations show that the proposed spin-exchange mechanism represents a valid candidate to realize fast quantum op-

Step 1: pulse 1,2,3
2-atom entanglement
A1 B1 C1 D1 A2 B2 C2 D2 A3 B3 C3 D3
Step 2: pulse 4,5,6
2-atom entanglement
A1 B1 C1 D1 A2 B2 C2 D2 A3 B3 C3 D3
Step 3: pulse 7,8,9
SWAP-like gate
A1 B1 C1 D1 A2 B2 C2 D2 A3 B3 C3 D3
Step 4: pulse 10,11,12
SWAP-like gate
A1 B1 C1 D1 A2 B2 C2 D2 A3 B3 C3 D3

FIG. 5: (Color online) Schematic illustration of a protocol to generating entanglement between 12 ^{87}Rb atoms loaded in a one-dimensional lattice. The pairwise entanglement protocol creates entanglement between atoms A_j and B_j (C_j and D_j) during step 1 (2), while the SWAP-like gate protocol entangles atoms B_j and C_j (D_j and A_{j+1}) during step 3 (4).

erations with Rydberg atoms.

VI. CONCLUSION

Throughout this work we have considered the case of individually trapped atoms addressed by external lasers. An interesting alternative realization of these protocols relies on the creation of a small *super-atom* in an elongated ensemble. This option has the advantage of solving the probabilistic loading of the individual traps as well as to provide a boost to the single-atom procedure by a factor $\sqrt{N}$ where N is the number of individual atoms in the super-atom. Quantum gates between super-atoms have been recently proposed [28] and the multiplexing of different qubits in an elongated ensemble has already been realized experimentally [32].

In conclusion, we have proposed a fast and robust mechanism to entangle neutral atoms. It is based on a variation of the van der Waals interaction between atoms excited to Rydberg states: for different principal quantum numbers, the spin-exchange interaction may be comparable to the Rydberg blockade shift thus induce a resonance between ground state levels and an entangled Rydberg state. This metastable state may then be mapped to a stable, entangled ground state. Furthermore, the entanglement efficiency may be improved by using small ensembles as well as by manipulating the structure of the Rydberg manifolds via external fields. Based on the spin-exchange interaction, pairwise entanglement along with a SWAP-like gate form the basis of a protocol for the generation of ground-state entanglement of many atoms in a chain configuration. These protocols may be implemented in present experiments leading to quantum manipulation of many-body systems.

Acknowledgments

XFS and TABK acknowledge support from AFOSR and the Quantum Memories MURI of the Air Force Office of Scientific Research. FB acknowledges support from the DARPA QuASAR program and the US NSF.

Appendix A: Single-atom optical excitation

This section shows how to realize the transitions in Fig 1(b) of the main text. We consider an atom optically excited via two linearly polarized light fields, one $\mathbf{x}$-polarized, the other $\mathbf{y}$-polarized, traveling along $\mathbf{y}$ and $\mathbf{x}$ direction, respectively. To have such a pair of light fields, a beam splitter is placed along the $\mathbf{z}$ axis as shown in Fig. 6. For each incoming light field, the following optical devices are used, (O_1), beam splitter, (O_2) and (O_3), mirror, and (O_4), a quarter-wave plate, or a wave plate whose thickness makes it effectively a combination of a half wave-plate and a quarter-wave plate, depending on the specific low-lying intermediate P state. By tuning the positions of the two mirrors so that they are symmetric to each other about the plane of the beam splitter, we have

$$l \equiv l_{12} + l_{25} = l_{13} + l_{35}, \tag{A1}$$

where $l_{\alpha\beta}$ is the distance between O_α and O_β, where $\alpha\ (\beta) = 1, \cdots, 5$. Here O_5 denotes the position of the atom. Assuming that the light field impinging on the beam splitter is $\mathbf{x}\mathscr{E}\cos(\omega t)$, one can show that the electric field on the atom is:

$$\mathbf{E} = -\frac{\mathscr{E}}{2\sqrt{2}}\left[\left(\mathbf{x} + \mathbf{y}e^{i\theta}\right)e^{i\omega t - ilk} + \text{h.c.}\right]. \tag{A2}$$

In order to excite the the Rydberg states $|\Uparrow\rangle$ and $|\Downarrow\rangle$ defined in the main text for either atom A or atom B, one shall use waveplates so that $\theta = \pi/2$ and $3\pi/2$, respectively. As a result, the transition from the ground level $|\uparrow\ (\downarrow)\rangle \equiv |5^2S_{\frac{1}{2}}, F = 2, m_F = 2(-1)\rangle$ to the Rydberg level $|\Downarrow\ (\Uparrow)\rangle \equiv |n\ ^2S_{\frac{1}{2}}, m_J = \mp 1/2, m_I = 1/2\rangle$ via an intermediate level $|6^2S_{\frac{1}{2}}, F = 1, m_F = 1\rangle$ ($|5^2S_{\frac{1}{2}}, F = 1, m_F = 0\rangle$) can be realized by a two-photon Rabi process via a pair of effective left (right)-hand polarized light fields.

The non-interacting Hamiltonian for atom A (the Hamiltonian for atom B is similar) in the dipole approximation and rotating-wave approximation for the atom-

field coupling is

$$
\begin{aligned}
H_{\rm A} &= \sum_{m_F} E_g|5S_{1/2},F=2,m_F\rangle\langle 5S_{1/2},F=2,m_F| \\
&+\sum_{m_f} E_{5e}|5P_{1/2},F'=1,m_f\rangle\langle 5P_{1/2},F'=1,m_f| \\
&+\sum_{m_f} E_{6e}|6P_{1/2},F'=1,m_f\rangle\langle 6P_{1/2},F'=1,m_f| \\
&+\Big[\sum_{m_J,m_I} E_r|m_J,m_I\rangle\langle m_J,m_I| \\
&+\sum_{m_F}\sum_{m_f}\Omega^{(ge)}_{5m_f,m_F}(q)e^{-i\omega_5^{(ge)}t} \\
&|5P_{1/2},F'=1,m_f\rangle\langle 5S_{1/2},F=2,m_F| \\
&+\sum_{m_f}\sum_{m_J,m_I}\Omega^{(er)}_{5m_f,m_Jm_I}(q)e^{i\omega_5^{(er)}t} \\
&|5P_{1/2},F'=1,m_f\rangle\langle m_J,m_I| \\
&+\sum_{m_F}\sum_{m_f}\Omega^{(ge)}_{6m_f,m_F}(\overline{q})e^{-i\omega_6^{(ge)}t} \\
&|6P_{1/2},F'=1,m_f\rangle\langle 5S_{1/2},F=2,m_F| \\
&+\sum_{m_f}\sum_{m_J,m_I}\Omega^{(er)}_{6m_f,m_Jm_I}(\overline{q})e^{i\omega_6^{(er)}t} \\
&|6P_{1/2},F'=1,m_f\rangle\langle m_J,m_I|+\text{h.c.}\Big], \qquad \text{(A3)}
\end{aligned}
$$

where $q=1(-1)$ indicates right (left)-hand polarization, E_j with $j=[g,5e,6e,r]$ is the energy of a specific atomic manifold, $\omega^{(ge)}_{5(6)}$ and $\omega^{(er)}_{5(6)}$ are the central frequencies of the lasers for the lower and upper transitions, and they satisfy

$$
\omega_5^{(ge)}+\omega_5^{(er)} = \omega_6^{(ge)}+\omega_6^{(er)}. \qquad \text{(A4)}
$$

The Rabi frequencies read,

$$
\begin{aligned}
\Omega^{(ge)}_{nm_f,m_F}(q) &= \frac{1}{2}D_n^{(ge)}\mathcal{E}_{ge}C^{F\ 1\ F'}_{m_F\ q\ m_f}, \\
\Omega^{(er)}_{nm_f,m_Jm_I}(\overline{q}) &= \frac{1}{2}D_n^{(er)}\mathcal{E}_{er}\sum_{\alpha}C^{\frac{1}{2}\ 1\ \frac{1}{2}}_{m_J\ \overline{q}\ \alpha}C^{\frac{1}{2}\ I\ F'}_{\alpha\ m_I\ m_f},
\end{aligned}
$$

where $n=5$ or 6, $\mathcal{E}_{ge(er)}$ is the electric field of the laser for the lower (upper) transition in Eq. (A2), $D_n^{(ge)}=e(nP_{1/2},F=1||r||5S_{1/2},F=2)$ and $D_n^{(er)}=e(nP_{1/2}||r||n_{\rm A}S_{1/2})$ are the reduced matrix elements of the electric dipole operator obtained via the Wigner-Eckart theorem [33, 34], with e the elementary charge,

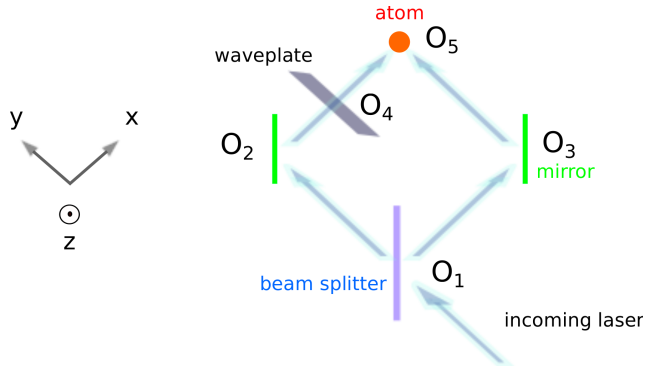

FIG. 6: (Color online) Schematic illustration for generating an effective right-hand or left-hand polarized light field from two linearly polarized light fields related by a $\pi/2$ or $3\pi/2$ phase difference.

and C a Clebsch-Gordan coefficient [33].

$$
\begin{aligned}
\frac{\Omega_n^{(ge)}(1)}{D_n^{(ge)}\mathcal{E}_{ge}} &= -\begin{pmatrix} 0.775 & 0 & 0 & 0 & 0 \\ 0 & 0.548 & 0 & 0 & 0 \\ 0 & 0 & 0.316 & 0 & 0 \end{pmatrix}, \\
\frac{\Omega_n^{(ge)}(-1)}{D_n^{(ge)}\mathcal{E}_{ge}} &= \begin{pmatrix} 0 & 0 & 0.316 & 0 & 0 \\ 0 & 0 & 0 & 0.548 & 0 \\ 0 & 0 & 0 & 0 & 0.775 \end{pmatrix}, \\
\frac{\Omega_n^{(er)}(1)}{D_n^{(er)}\mathcal{E}_{er}} &= -\begin{pmatrix} 0 & 0 & 0 & 0 & 0 & 0.408 & 0 & 0 \\ 0 & 0 & 0 & 0 & 0 & 0 & 0.577 & 0 \\ 0 & 0 & 0 & 0 & 0 & 0 & 0 & 0.707 \end{pmatrix}, \\
\frac{\Omega_n^{(er)}(-1)}{D_n^{(er)}\mathcal{E}_{er}} &= \begin{pmatrix} 0.707 & 0 & 0 & 0 & 0 & 0 & 0 & 0 \\ 0 & 0.577 & 0 & 0 & 0 & 0 & 0 & 0 \\ 0 & 0 & 0.408 & 0 & 0 & 0 & 0 & 0 \end{pmatrix}.
\end{aligned}
$$

Here, the column and row indices for $\Omega^{(ge)}$ are for quantum numbers $m_F=[-2,-1,0,1,2]$ (from left to right) and $m_f=[-1,0,1]$ (from top to bottom), and the column and row indices for $\Omega^{(er)}$ are for quantum numbers $(m_Jm_I)=[(\frac{-1}{2}\frac{-3}{2}),(\frac{-1}{2}\frac{-1}{2}),(\frac{-1}{2}\frac{1}{2}),(\frac{-1}{2}\frac{3}{2}),(\frac{1}{2}\frac{-3}{2}),(\frac{1}{2}\frac{-1}{2}),(\frac{1}{2}\frac{1}{2}),(\frac{1}{2}\frac{3}{2})]$(from left to right) and $m_f=[-1,0,1]$(from top to bottom).

Below, we derive the effective two-photon Rabi frequency when the two-photon detuning is zero [35–37]. Using the method of Ref. [35], we can derive a Hamiltonian for far off resonant optical driving. The method of Ref. [35] is essentially an adiabatic approximation. The Hamiltonian in a rotating frame and rotating-wave approximation for a three level system with basis $|r\rangle$, $|e\rangle$, $|g\rangle$ is (the subscripts d and u denote down and up, respectively)

$$
H_{\rm 3level} = \begin{pmatrix} 0 & e^{ik_{\rm u}l_{\rm u}}\Omega_{\rm u}/2 & 0 \\ e^{-ik_{\rm u}l_{\rm u}}\Omega_{\rm u}/2 & -\Delta & e^{ik_{\rm d}l_{\rm d}}\Omega_{\rm d}/2 \\ 0 & e^{-ik_{\rm d}l_{\rm d}}\Omega_{\rm d}/2 & 0 \end{pmatrix},
$$

where $l_{\rm u(d)}$ is the length defined in Eq. (A1) for the tran-

sition from $|g\rangle$ to $|e\rangle$ (from $|e\rangle$ to $|r\rangle$). Here we assume that $\Omega_{\rm u(d)}$ is real, and the two-photon transition is resonant. We write the wave function as $\alpha_r|r\rangle+\alpha_e|e\rangle+\alpha_g|g\rangle$, and starting from state $(\alpha_r(0),\alpha_g(0))=(0,1)$, one can find $|\alpha_r(t)|\leq\frac{|\Omega_{\rm d}\Omega_{\rm u}|}{\Omega_{\rm d}^2+\Omega_{\rm u}^2}\leq 1$ and

$$|\alpha_g(t)|^2 \;=\; 1+\frac{2\Omega_{\rm d}^2\Omega_{\rm u}^2}{(\Omega_{\rm d}^2+\Omega_{\rm u}^2)^2}\left[\cos\frac{t\left(\Omega_{\rm d}^2+\Omega_{\rm u}^2\right)}{4\Delta}-1\right],$$

which indicates that $\mathrm{Max}|\alpha_g(t)|^2$ and $\mathrm{Min}|\alpha_g(t)|^2$ achieve maximum difference only when $|\Omega_{\rm d}|=|\Omega_{\rm u}|$. This can guide setting up the condition in experiments. In fact, when the difference of $\mathrm{Max}|\alpha_g(t)|^2$ and $\mathrm{Min}|\alpha_g(t)|^2$ reaches its maximum while adjusting one of $|\Omega_{\rm d}|,|\Omega_{\rm u}|$, the condition $|\Omega_{\rm d}|=|\Omega_{\rm u}|$ is met. When $\Omega_{\rm d}=\Omega_{\rm u}$, the Hamiltonian in a rotating frame is

$$H \;=\; \frac{\Omega_{\rm d}\Omega_{\rm u}}{4\Delta}\begin{pmatrix}0 & e^{i(k_{\rm d}l_{\rm d}+k_{\rm u}l_{\rm u})}\\ e^{-i(k_{\rm d}l_{\rm d}+k_{\rm u}l_{\rm u})} & 0\end{pmatrix}.$$

When the lower and upper Rabi transitions have the same Rabi frequency, the effective Rabi frequency between $|r\rangle$ and $|g\rangle$ is $\frac{\Omega_{\rm d}\Omega_{\rm u}}{2\Delta}e^{i(k_{\rm d}l_{\rm d}+k_{\rm u}l_{\rm u})}$. By assuming $\frac{\Omega_{\rm d}\Omega_{\rm u}}{2\Delta}>0$, we can write the effective Rabi frequency as $|\frac{\Omega_{\rm d}\Omega_{\rm u}}{2\Delta}|e^{i(k_{\rm d}l_{\rm d}+k_{\rm u}l_{\rm u})}$.

For the system studied in the main text, we shall identify $k_{\rm d}l_{\rm d}+k_{\rm u}l_{\rm u}$ as $-\phi_{\rm A}$ for the two-photon transition via 5P state of atom A, while as $-\phi^{\rm A}$ for the two-photon transition via 6P state of atom A. But since both of these two-photon transitions are resonant, and the ground states or the Rydberg states are degenerate, we immediately find $\phi_\alpha=\phi^\alpha$ if one sets a common $l\equiv l_{\rm d}=l_{\rm u}$ for exciting both of the two Rydberg state $|\Uparrow\rangle_\alpha$ and $|\Downarrow\rangle_\alpha$, with $\alpha=A$ or B.

Appendix B: van der Waals interaction

Since we consider the uncommon situation of the interaction between two Rydberg levels of different principal quantum numbers, we will briefly outline a perturbation calculation here. Consider two ^{87}Rb Rydberg atoms, one prepared in state $|r_{1\pm}\rangle=|n_1\ {}^2S_{\frac{1}{2}},m_J=\pm1/2\rangle$, and the other in state $|r_{2\pm}\rangle=|n_2\ {}^2S_{\frac{1}{2}},m_J=\pm1/2\rangle$, where $n_1\neq n_2$. We consider the following four channels for the dipole-dipole interaction, each characterized by its energy defect [29],

$$\begin{aligned}
\delta_1(n_s,n_t) &= E(n_sp_{\frac{3}{2}})+E(n_tp_{\frac{3}{2}})-E(n_1s_{\frac{1}{2}})-E(n_2s_{\frac{1}{2}}),\\
\delta_2(n_s,n_t) &= E(n_sp_{\frac{3}{2}})+E(n_tp_{\frac{1}{2}})-E(n_1s_{\frac{1}{2}})-E(n_2s_{\frac{1}{2}}),\\
\delta_3(n_s,n_t) &= E(n_sp_{\frac{1}{2}})+E(n_tp_{\frac{3}{2}})-E(n_1s_{\frac{1}{2}})-E(n_2s_{\frac{1}{2}}),\\
\delta_4(n_s,n_t) &= E(n_sp_{\frac{1}{2}})+E(n_tp_{\frac{1}{2}})-E(n_1s_{\frac{1}{2}})-E(n_2s_{\frac{1}{2}}).
\end{aligned}\tag{B1}$$

Here (n_s,n_t) denote the principal quantum numbers of the pair state produced by the scattering process. These four couplings are known to be the dominant ones in our case. In the van der Waals interaction the atoms then go back to the initial levels and the magnetic quantum number of either atom can change up to 1 unit [29]. We can separate the angular dependence of the interaction from the principal quantum numbers. Its matrix representation in the basis of $|r_{1+}r_{2+}\rangle,(|r_{1-}r_{2+}\rangle+|r_{1+}r_{2-}\rangle)/\sqrt{2},(|r_{1-}r_{2+}\rangle-|r_{1+}r_{2-}\rangle)/\sqrt{2},|r_{1-}r_{2-}\rangle$ is given by

$$\begin{aligned}
D_1 &= \mathrm{diag}(22,34,18,22)/81,\\
D_2 &= D_3=\mathrm{diag}(14,2,18,14)/81,\\
D_4 &= \mathrm{diag}(4,16,0,4)/81,
\end{aligned}\tag{B2}$$

where $\mathrm{diag}(a_1,a_2,a_3,a_4)$ means a diagonal matrix with a_i as diagonal matrix elements. In the basis of $|r_{1+}r_{2+}\rangle$,$|r_{1-}r_{2+}\rangle$, $|r_{1+}r_{2-}\rangle$, and $|r_{1-}r_{2-}\rangle$, Eq. (B2) becomes,

$$\begin{aligned}
D(\delta_1) &= \frac{1}{81}\begin{pmatrix}22&0&0&0\\0&26&8&0\\0&8&26&0\\0&0&0&22\end{pmatrix},\\
D(\delta_{2(3)}) &= \frac{1}{81}\begin{pmatrix}14&0&0&0\\0&10&-8&0\\0&-8&10&0\\0&0&0&14\end{pmatrix},\\
D(\delta_4) &= \frac{1}{81}\begin{pmatrix}4&0&0&0\\0&8&8&0\\0&8&8&0\\0&0&0&4\end{pmatrix}.
\end{aligned}$$

The van der Waals interaction strength for each channel is

$$C_6^{(k)} \;=\; \sum_{\Delta n_{\rm A},\Delta n_{\rm B}=-\Delta n}^{\Delta n}\mathcal{C}_6(\delta_k(n_{\rm A}+\Delta n_{\rm A},n_{\rm B}+\Delta n_{\rm B})).$$

We can identify two types of $\mathcal{C}_6$ coefficients:

$$\begin{aligned}
&\mathcal{C}_6(\delta_k)=\frac{-e^4}{\delta_i(n_{\rm A}+\Delta n_{\rm A},n_{\rm B}+\Delta n_{\rm B})}\\
&\left(\int rP_{n_{\rm A},l_{\rm A}}P_{n_{\rm A}+\Delta n_{\rm A},l'_{\rm A}}dr\int rP_{n_{\rm B},l_{\rm B}}P_{n_{\rm B}+\Delta n_{\rm B},l'_{\rm B}}dr\right)^2,\\
&\mathcal{C}'_6(\delta_k)=\frac{-e^4}{\delta_i(n_{\rm A}+\Delta n_{\rm A},n_{\rm B}+\Delta n_{\rm B})}\\
&\int rP_{n_{\rm A},l_{\rm A}}P_{n_{\rm A}+\Delta n_{\rm A},l'_{\rm A}}dr\int rP_{n_{\rm B},l_{\rm B}}P_{n_{\rm B}+\Delta n_{\rm B},l'_{\rm B}}dr\\
&\int rP_{n_{\rm B},l_{\rm B}}P_{n_{\rm A}+\Delta n_{\rm A},l'_{\rm A}}dr\int rP_{n_{\rm A},l_{\rm A}}P_{n_{\rm B}+\Delta n_{\rm B},l'_{\rm B}}dr,
\end{aligned}\tag{B3}$$

with $i=1,2,3$ or 4. Here $P_{n_{1(2)},l_{1(2)}}$ is the radial part of the atomic wave function, and the integration about

Value of Δn	$C_6^{(2)}$ ($C_6^{(3)}$)
1	71841.8
2	71922.5
3	71928.5
6	71929.9
10	71930
15	71930
20	71930

TABLE II: Convergence of the van der Walls interaction strength depending on the channels considered (up to Δn) for a pair of atoms in the state $|100^2S_{\frac{1}{2}}\rangle$. Unit: GHz$\mu$m^6.

$P_{n_{1(2)},l_{1(2)}}$ can be approximated as in Ref. [31]. When $n_1 = n_2$, we have $\mathcal{C}_6 = \mathcal{C}_6'$. Also, the two channels with energy defect δ_2 and δ_3 are the same. We report in Table II the values of $C_6^{(2)}$ or $C_6^{(3)}$ for different Δn for two atoms at $n_1 = n_2 = 100, l_1 = l_2 = 0$. The total van der Waals interaction $\sum_x C_6^{(x)} D_x/(2\pi)$ is

$$\hat{H}_{\rm vdW}^{(100,100)} = \begin{pmatrix} 56200 & 0 & 0 & 0 \\ 0 & 56980 & 1573 & 0 \\ 0 & 1573 & 56980 & 0 \\ 0 & 0 & 0 & 56200 \end{pmatrix} \frac{\mu\text{m}^6\text{GHz}}{L^6}, \tag{B4}$$

where L is the distance between the two atoms. The van der Waals interaction for two atoms in the $n_1 = 97, n_2 = 100, l_1 = l_2 = 0$ levels shall be calculated considering that the two atoms may swap their principal quantum numbers, i.e., we shall take into account the two cases with $\mathcal{C}_6$ and $\mathcal{C}_6'$. The calculation gives us

$$\hat{H}_{\rm vdW}^{(97,100)} = \begin{pmatrix} \hat{V}_1 & \hat{V}_2 \\ \hat{V}_2 & \hat{V}_1 \end{pmatrix}, \tag{B5}$$

where

$$\hat{V}_1 = -\begin{pmatrix} 89180 & 0 & 0 & 0 \\ 0 & 59780 & -58800 & 0 \\ 0 & -58800 & 59780 & 0 \\ 0 & 0 & 0 & 89180 \end{pmatrix} \frac{\mu\text{m}^6\text{GHz}}{L^6},$$

$$\hat{V}_2 = \begin{pmatrix} -537 & 0 & 0 & 0 \\ 0 & -375 & 324 & 0 \\ 0 & 324 & -375 & 0 \\ 0 & 0 & 0 & -537 \end{pmatrix} \frac{\mu\text{m}^6\text{GHz}}{L^6}, \tag{B6}$$

and the basis vectors of $\hat{H}_{\rm vdW}^{(97,100)}$ for the columns from left to right, and for the rows from top to bottom are

$$|r_{\text{A}+}r_{\text{B}+}\rangle, |r_{\text{A}-}r_{\text{B}+}\rangle, |r_{\text{A}+}r_{\text{B}-}\rangle, |r_{\text{A}-}r_{\text{B}-}\rangle, |r_{\text{B}+}r_{\text{A}+}\rangle, |r_{\text{B}-}r_{\text{A}+}\rangle, |r_{\text{B}+}r_{\text{A}-}\rangle, |r_{\text{B}-}r_{\text{A}-}\rangle. \tag{B7}$$

From this matrix, we find that the transition rate to a pair state with exchanged quantum numbers is only 0.6% of that to a state pair with the same quantum numbers. Thus, we can safely ignore these terms. In this approximation, the van der Waals interaction is, in the basis of $|r_{1+}r_{2+}\rangle, |r_{1-}r_{2+}\rangle, |r_{1+}r_{2-}\rangle, |r_{1-}r_{2-}\rangle$

$$\hat{H}_{\rm vdW}^{(97,100)} \approx \begin{pmatrix} \hat{V}_1 & 0 \\ 0 & \hat{V}_1 \end{pmatrix}. \tag{B8}$$

In the two-atom product basis $|r_{\text{A}-}r_{\text{B}+}\rangle$, $|r_{\text{A}+}r_{\text{B}-}\rangle$, the total van der Waals interaction is then,

$$\hat{H}_{\rm v} = \frac{1}{L^6}\begin{pmatrix} C_6 & C_6^{\rm ex} \\ C_6^{\rm ex} & C_6 \end{pmatrix}, \tag{B9}$$

where the four matrix elements are given in $\hat{V}_1$ of Eq. (B6) for the case of $n_{\rm A} = 97, n_{\rm B} = 100$. This implies that $C_6/(2\pi) = -59780$ [GHz μm^6] and $C_6^{\rm ex}/(2\pi) = 58800$ [GHz μm^6] in the main text.

1. Critical radius for van der Waals interaction

Since we derive the van der Waals strength via a perturbative calculation based on the dipole-dipole potential, it is useful to study the transition from the dipole-dipole interaction to the van der Waals interaction. We consider the relevant case of $n_1 = 97, n_2 = 100, l_1 = l_2 = 0$ again. From Ref. [29], the dipole-dipole interaction can be written as

$$V_{n_1,n_2}^{\rm dd} = R_{\rm rr} M_{j_1' m_1' j_2' m_2'; j_1 m_1 j_2 m_2}/\mathcal{L}^3, \tag{B10}$$

where M is a matrix characterizing the angular dependence of the interaction [29], and

$$R_{\rm rr} = e^2 \int r P_{n_1,l_1} P_{n_1+\Delta n_1, l_1'} dr \int r P_{n_2,l_2} P_{n_2+\Delta n_2, l_2'} dr.$$

The coefficient $R_{\rm rr}$ is closely related to the usual C_3 matrix element. In Table III, all the two-atom Rydberg p-states with an energy defect δ_e smaller than 1 GHz with respect to the state $n_1 = 97, n_2 = 100, l_1 = l_2 = 0$, and $R_{\rm rr}$ larger than 1 GHzμm^3 are listed, from which one finds that the condition $\Delta n_1 = 0$ (2), $\Delta n_2 = -1(-3)$ gives the smallest energy defects. Since for $\Delta n_1 = 2, \Delta n_2 = -3$, the radial matrix elements are small, we consider the case $\Delta n_1 = 0, \Delta n_2 = -1$, where we find

$$M(\delta_1) = \begin{pmatrix} 0 & 0 & 0 & 0 \\ 0 & 0 & 0 & 0 \\ -0.19 & 0 & 0 & 0 \\ 0 & -0.33 & 0 & 0 \\ 0 & 0 & 0 & 0 \\ -0.44 & 0 & 0 & 0 \\ 0 & -0.44 & -0.11 & 0 \\ 0 & 0 & 0 & -0.19 \\ -0.19 & 0 & 0 & 0 \\ 0 & -0.11 & -0.44 & 0 \\ 0 & 0 & 0 & -0.44 \\ 0 & 0 & 0 & 0 \\ 0 & 0 & -0.33 & 0 \\ 0 & 0 & 0 & -0.19 \\ 0 & 0 & 0 & 0 \\ 0 & 0 & 0 & 0 \end{pmatrix}, \quad \text{(B11)}$$

$$M(\delta_{2(3)}) = \begin{pmatrix} 0 & 0 & 0 & 0 \\ -0.27 & 0 & 0 & 0 \\ -0.31 & 0 & 0 & 0 \\ 0 & 0.31 & -0.16 & 0 \\ 0 & 0.16 & -0.31 & 0 \\ 0 & 0 & 0 & 0.31 \\ 0 & 0 & 0 & 0.27 \\ 0 & 0 & 0 & 0 \end{pmatrix}, \quad \text{(B12)}$$

$$M(\delta_4) = \begin{pmatrix} -0.22 & 0 & 0 & 0 \\ 0 & 0.22 & 0.22 & 0 \\ 0 & 0.22 & 0.22 & 0 \\ 0 & 0 & 0 & -0.22 \end{pmatrix}, \quad \text{(B13)}$$

where the column indices for the three matrices are $(m_1, m_2) = [(\frac{-1}{2}, \frac{-1}{2}), (\frac{-1}{2}, \frac{1}{2}), (\frac{1}{2}, \frac{-1}{2}), (\frac{1}{2}, \frac{1}{2})]$ from left to right, and the row indices are $(m_1', m_2') = [(-j_1', -j_2'), (-j_1', -j_2'+1), \cdots, (j_1', j_2'-1), (j_1', j_2')]$ from top to bottom. From the three matrices and Table III, we find that the state $(97p_{1/2}, 99p_{3/2})$ is the dominant scattering channel and we can thus determine the critical distance $L_{\text{dd-vdW}}$ where dipole-dipole interaction transitions into the van der Waals regime,

$$\text{Max}(MR_{\text{rr}})/L^3_{\text{dd-vdW}} = |\delta_e|, \quad \text{(B14)}$$

where $\text{Max}(\cdots)$ denotes the maximum matrix element for the dipole-dipole interaction, and δ_e is the energy defect of the state $(97p_{1/2}, 99p_{3/2})$. This gives $L_{\text{dd-vdW}} \approx 9.6\mu$m. In order to implement efficiently the entanglement protocol in the main text, we may set $L > 20\mu$m. In particular, for $L = 26\mu$m, the matrix $\hat{V}_1$ in Eq. (B6) becomes

$$\hat{V}_1^{(97,100)} = -\begin{pmatrix} 289 & 0 & 0 & 0 \\ 0 & 194 & -190 & 0 \\ 0 & -190 & 194 & 0 \\ 0 & 0 & 0 & 289 \end{pmatrix} \text{kHz}.$$

atom 1	atom 2	δ_e (MHz)	R_{rr} (GHzμm^3)
$96p_{1/2}$	$100p_{1/2}$	-779	98.3
$96p_{1/2}$	$100p_{3/2}$	-685	96.8
$96p_{3/2}$	$100p_{1/2}$	-672	100.1
$96p_{3/2}$	$100p_{3/2}$	-578	98.5
$97p_{1/2}$	$99p_{1/2}$	-62	98.4
$97p_{1/2}$	$99p_{3/2}$	35	100.2
$97p_{3/2}$	$99p_{1/2}$	42	96.8
$97p_{3/2}$	$99p_{3/2}$	139	98.6
$98p_{1/2}$	$98p_{1/2}$	177	1.7
$98p_{1/2}$	$98p_{3/2}$	277	1.6
$98p_{3/2}$	$98p_{1/2}$	277	1.7
$98p_{3/2}$	$98p_{3/2}$	378	1.7

TABLE III: Table of relevant scattering channels via dipole-dipole interaction for a pair state with $n_1 = 97, n_2 = 100, l_1 = l_2 = 0$.

The same analysis for the pair state $n_1 = 73, n_2 = 75, l_1 = l_2 = 0$, with relevant energy defects and R_{rr} listed in Table IV, gives a critical distance 6.1μm. We may set $L = 15\mu$m, then the interaction matrix is

$$\hat{V}_1^{(73,75)} = \begin{pmatrix} 535 & 0 & 0 & 0 \\ 0 & 358 & -353 & 0 \\ 0 & -353 & 358 & 0 \\ 0 & 0 & 0 & 535 \end{pmatrix} \text{kHz}.$$

The occurrence of a strong spin-exchange interaction in these cases arises through an interference effect involving a small number of dominant intermediate $p_{1/2}$ and $p_{3/2}$ states. From Table III and IV, one finds that the strong spin-exchange interaction comes from the dominating scattering channels with energy defects $\delta_2(n_s, n_t)$ and $\delta_3(n_s, n_t)$ in Eq. (B1). If we only consider the two dominating channels $73p_{1/2}, 74p_{3/2}$ and $73p_{3/2}, 74p_{1/2}$ for two atoms with principal quantum number 73 and 75, then $V_+ : V_- = 1 : 9$ from Eq. (B2). The channel that contributes next strongly comparing to these two channels is $73p_{3/2}, 74p_{3/2}$, whose energy defect has a sign difference to those of $73p_{1/2}, 74p_{3/2}$ and $73p_{3/2}, 74p_{1/2}$. So, from Eq. (B2), if we consider only this channel with its contribution to the blockade V_+' and V_-', then $V_+' : V_-' = -17 : -9$, which will reduce V_+ furthermore, giving a negligible V_+ comparing to V_-. For two atoms with principal quantum numbers 97 and 100, there are two dominating scattering channels $97p_{1/2}, 99p_{3/2}$ and $97p_{3/2}, 99p_{1/2}$. With only these two channels, we shall have $V_+ : V_- = -1 : -9$. The channel that contributes next strongly comparing to them is $97p_{1/2}, 99p_{1/2}$. If we consider only this channel, then $V_+' > 0 = V_-'$, which will reduce V_+ furthermore, giving $|V_+/V_-| < 1/9$.

atom 1	atom 2	δ_e (MHz)	$R_{\rm rr}$ (GHzμm^3)
$73p_{1/2}$	$74p_{3/2}$	-51	30.5
$73p_{3/2}$	$74p_{1/2}$	-41	29.5
$73p_{3/2}$	$74p_{3/2}$	198	30.1
$74p_{1/2}$	$73p_{1/2}$	-291	0.5
$74p_{1/2}$	$73p_{3/2}$	-41	0.5
$74p_{3/2}$	$73p_{1/2}$	-51	0.5
$74p_{3/2}$	$73p_{3/2}$	198	0.5

TABLE IV: Table of relevant scattering channels via dipole-dipole interaction for a pair state with $n_1 = 73, n_2 = 75, l_1 = l_2 = 0$.

Appendix C: State evolution during Pulse 2

Pulse 2 consists of a two-photon excitation of atom B with effective Rabi frequency $\Omega^{\rm B}$. This pulse excites $|\uparrow\rangle$ to $|\Downarrow\rangle$ via the $6P$ state as in Fig. 1(b). By writing the state vector as $\alpha_{\overline{rg}}|\Uparrow\uparrow\rangle + \alpha_{r_+}|r_+\rangle + \alpha_{r_-}|r_-\rangle$, the time evolution is given by

$$i\frac{d}{dt}\begin{pmatrix}\alpha_{\overline{rg}}\\ \alpha_{r_+}\\ \alpha_{r_-}\end{pmatrix} = \begin{pmatrix}0 & \Omega_1 & \Omega_1\\ \Omega_1 & V_+ & 0\\ \Omega_1 & 0 & V_-\end{pmatrix}\begin{pmatrix}\alpha_{\overline{rg}}\\ \alpha_{r_+}\\ \alpha_{r_-}\end{pmatrix}, \quad \text{(C1)}$$

where $\Omega_1 = \Omega^{\rm B}/(2\sqrt{2})$. In the equation above, we have $|V_-| \gg |V_+|, \Omega_1$. Then at the time

$$\tau_2 = \frac{\pi}{\sqrt{V_+^2 + 4\Omega_1^2 - \frac{4\Omega_1^3}{V_-}}} \approx \frac{\pi}{2\Omega_1}\left[1 - \frac{V_+^2}{8\Omega_1^2}\right], \quad \text{(C2)}$$

the population on the Rydberg Bell state is maximal

$$|\alpha_{r_+}| = \frac{2\Omega_1}{\sqrt{V_+^2 + 4\Omega_1^2 - \frac{4\Omega_1^3}{V_-}}} \approx 1 - \frac{V_+^2}{[\Omega^{\rm B}]^2}. \quad \text{(C3)}$$

Appendix D: State evolution during Pulse 3

As analyzed in the main text, there are 8 states relevant to the dynamics of pulse 3. We write the wavefunction for the system as

$$\begin{aligned}|\psi\rangle = {} & \alpha_{\underline{g\overline{g}}}|m_F^{(\rm A)} = -1; m_F^{(\rm B)} = 2\rangle\\ & + \alpha_{\overline{g}\underline{g}}|m_F^{(\rm A)} = 2; m_F^{(\rm B)} = -1\rangle\\ & + \alpha_{\underline{gr}}|m_F^{(\rm A)} = -1; R_-^{(\rm B)}\rangle + \alpha_{\overline{gr}}|m_F^{(\rm A)} = 2; R_+^{(\rm B)}\rangle\\ & + \alpha_{\underline{rg}}|R_-^{(\rm A)}; m_F^{(\rm B)} = -1\rangle + \alpha_{\overline{rg}}|R_+^{(\rm A)}; m_F^{(\rm B)} = 2\rangle\\ & + \alpha_{\overline{r}\underline{r}}|R_+^{(\rm A)}; R_-^{(\rm B)}\rangle + \alpha_{\underline{r}\overline{r}}|R_-^{(\rm A)}; R_+^{(\rm B)}\rangle, \end{aligned} \quad \text{(D1)}$$

where $|R_\pm^{(\alpha)}\rangle = |m_J^{(\alpha)} m_I^{(\alpha)} = \frac{\pm 1}{2}\frac{1}{2}\rangle$, then the dynamics is determined by the Schrödinger equation,

$$i\frac{d}{dt}\begin{pmatrix}\alpha_{\underline{g\overline{g}}}\\ \alpha_{\overline{g}\underline{g}}\\ \alpha_{\underline{gr}}\\ \alpha_{\overline{gr}}\\ \alpha_{\underline{rg}}\\ \alpha_{\overline{rg}}\\ \alpha_{\underline{r}\overline{r}}\\ \alpha_{\overline{r}\underline{r}}\end{pmatrix} = \frac{1}{2}\begin{pmatrix}0 & 0 & \Omega^{\rm B}e^{i\phi^{\rm B}} & 0 & 0 & \Omega_{\rm A}e^{i\phi_{\rm A}} & 0 & 0\\ 0 & 0 & 0 & \Omega_{\rm B}e^{i\phi_{\rm B}} & \Omega^{\rm A}e^{i\phi^{\rm A}} & 0 & 0 & 0\\ \Omega^{\rm B}e^{-i\phi^{\rm B}} & 0 & 0 & 0 & 0 & 0 & 0 & \Omega_{\rm A}e^{i\phi_{\rm A}}\\ 0 & \Omega_{\rm B}e^{-i\phi_{\rm B}} & 0 & 0 & 0 & 0 & \Omega^{\rm A}e^{i\phi^{\rm A}} & 0\\ 0 & \Omega^{\rm A}e^{-i\phi^{\rm A}} & 0 & 0 & 0 & 0 & \Omega_{\rm B}e^{i\phi_{\rm B}} & 0\\ \Omega_{\rm A}e^{-i\phi_{\rm A}} & 0 & 0 & 0 & 0 & 0 & 0 & \Omega^{\rm B}e^{i\phi^{\rm B}}\\ 0 & 0 & 0 & \Omega^{\rm A}e^{-i\phi^{\rm A}} & \Omega_{\rm B}e^{-i\phi_{\rm B}} & 0 & 2V_{\rm s} & 2V_{\rm c}\\ 0 & 0 & \Omega_{\rm A}e^{-i\phi_{\rm A}} & 0 & 0 & \Omega^{\rm B}e^{-i\phi^{\rm B}} & 2V_{\rm c} & 2V_{\rm s}\end{pmatrix}\begin{pmatrix}\alpha_{\underline{g\overline{g}}}\\ \alpha_{\overline{g}\underline{g}}\\ \alpha_{\underline{gr}}\\ \alpha_{\overline{gr}}\\ \alpha_{\underline{rg}}\\ \alpha_{\overline{rg}}\\ \alpha_{\underline{r}\overline{r}}\\ \alpha_{\overline{r}\underline{r}}\end{pmatrix}, \quad \text{(D2)}$$

where $V_{\rm s} = C_6/L^6$ and $V_{\rm c} = C_6^{ex}/L^6$. The Hamiltonian $\hat{H}_{\rm Pulse3}$ gives the following coupling

$$\begin{aligned}\langle\Uparrow\mathcal{B}|\hat{H}_{\rm Pulse3}|\downarrow\mathcal{B}\rangle &= \Omega_{\rm A}e^{-i\phi_{\rm A}},\\ \langle\Downarrow\mathcal{B}|\hat{H}_{\rm Pulse3}|\uparrow\mathcal{B}\rangle &= \Omega^{\rm A}e^{-i\phi^{\rm A}},\\ \langle\mathcal{A}\Uparrow|\hat{H}_{\rm Pulse3}|\mathcal{A}\downarrow\rangle &= \Omega_{\rm B}e^{-i\phi_{\rm B}},\\ \langle\mathcal{A}\Downarrow|\hat{H}_{\rm Pulse3}|\mathcal{A}\uparrow\rangle &= \Omega^{\rm B}e^{-i\phi^{\rm B}}, \end{aligned} \quad \text{(D3)}$$

where the phase factors have been defined previously and $\mathcal{A}$ and $\mathcal{B}$ represent an arbitrary state of atom A and B. With all the optical excitation channels active, the Rydberg state can be mapped down to the intermediate states $|\Uparrow\uparrow\rangle, |\Downarrow\downarrow\rangle$, $|\uparrow\Uparrow\rangle$, and $|\downarrow\Downarrow\rangle$, where for convenience

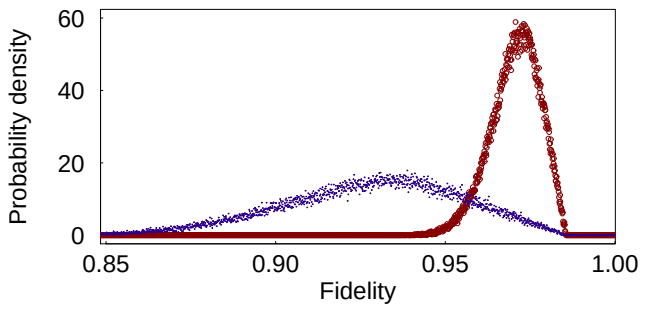

FIG. 7: (Color online) Probability distribution of fidelity for the ground Bell state when each of the four two-photon Rabi frequencies in pulse 3 obeys a uniform distribution in $[1-\epsilon,\ 1+\epsilon]\Omega$, where $\epsilon = 0.1$ (0.2) for the empty circle and dot.

we introduce new basis states

$$|\mathscr{U}_\pm\rangle \equiv \left[e^{i\phi^{\rm B}}|\Uparrow\uparrow\rangle \pm e^{i\phi^{\rm A}}|\uparrow\Uparrow\rangle\right]/\sqrt{2},$$
$$|\mathscr{D}_\pm\rangle \equiv \left[e^{i\phi_{\rm B}}|\Downarrow\downarrow\rangle \pm e^{i\phi_{\rm A}}|\downarrow\Downarrow\rangle\right]/\sqrt{2}. \quad \text{(D4)}$$

Then it is easily seen that only states $|\mathscr{U}_+\rangle$ and $|\mathscr{D}_+\rangle$ are coupled with entangled Rydberg state $|r_+\rangle$, while the other two states $|\mathscr{U}_-\rangle$ and $|\mathscr{D}_-\rangle$ are decoupled from $|r_+\rangle$ when the Rabi frequencies satisfy $\Omega \equiv \Omega_{\rm A} = \Omega^{\rm A} = \Omega_{\rm B} = \Omega^{\rm B}$. The states $|\mathscr{U}_+\rangle$ and $|\mathscr{D}_+\rangle$ are further coupled to the ground states $|\downarrow\uparrow\rangle$ and $|\uparrow\downarrow\rangle$. If we define the basis states

$$|\Phi_\pm\rangle \equiv \left[e^{i(\phi_{\rm A}+\phi^{\rm B})}|\downarrow\uparrow\rangle \pm e^{i(\phi^{\rm A}+\phi_{\rm B})}|\uparrow\downarrow\rangle\right]/\sqrt{2}, \quad \text{(D5)}$$

it is easy to show that only the state $|\Phi_+\rangle$ is coupled with $|\mathscr{U}_+\rangle$ and $|\mathscr{D}_+\rangle$. Hence only four states $|r_+\rangle$, $|\mathscr{U}_+\rangle$, $|\mathscr{D}_+\rangle$ and $|\Phi_+\rangle$ interact during pulse 3. When atom A is excited by four sets of light fields, each in the diamond-shaped configuration, we can have $\phi_{\rm A} = \phi^{\rm A}$; similarly for atom B. In this case, $|g_\pm\rangle = |\Phi_\pm\rangle$, up to overall phase, and we create a ground Bell state $|g_+\rangle$. We henceforth assume that $\phi_{\rm A} = \phi^{\rm A}$ and $\phi_{\rm B} = \phi^{\rm B}$ are satisfied, which justifies neglecting these phases in the main text for simplicity. The main practical difficulty is to set all four Rabi frequencies in Eq. (D2) or (D3) equal to each other. In order to show that the method proposed above is robust against dispersion in the Rabi frequencies, we numerically simulate the system evolution by independently varying $\Omega_{\rm A}, \Omega^{\rm A}, \Omega_{\rm B}$ and $\Omega^{\rm B}$ among the interval $[1-\epsilon,\ 1+\epsilon]\Omega$ (i.e., each Rabi frequency obeys a uniform distribution) for pulse 3, with $\Omega = \sqrt{V_+V_-}$, $\tau_2 = (\sqrt{2}\pi/\Omega)\left[1-(V_+/\Omega)^2\right]$, and $\tau_3 = \pi/\Omega$. By performing 10^5 such simulations, we find that almost all fidelities are larger than 95% (85%) for $\epsilon = 0.1$ (0.2), as shown in Fig. 7. We note that an almost identical robustness holds for the fidelity of preparation of $|\Phi_+\rangle$, as opposed to $|g_+\rangle$, in the case where the phases $\phi_{\rm A}, \phi^{\rm A}, \phi_{\rm B}$ and $\phi^{\rm B}$ in Eq. (D3) are chosen randomly.

Appendix E: Entanglement of atomic chains

In this section we describe in detail the entanglement of a one-dimensional chain of 4 and 6 atoms separated by a distance $L = 15\mu$m. We consider the following Rydberg target states: $n_1 = 73, l_1 = 0$ and $n_2 = 75, l_2 = 0$. The relevant Rydberg interaction between two nearest-neighboring atoms is characterized by the spin-exchange process:

$$V_+/(2\pi) \approx 5\text{kHz}, \quad V_-/(2\pi) \approx 700\text{kHz}. \quad \text{(E1)}$$

The strongest blockade interaction for non-neighboring atoms is

$$V_1^{(73,75)}(1,1)/(2\pi) = V_1^{(73,75)}(4,4)/(2\pi) \approx 0.7\text{kHz}. \quad \text{(E2)}$$

This means we can safely ignore the blockade effect due to multiple Rydberg excitations in the chain. Since the first and second steps in the entangling protocol shown in the main text is simply the entanglement between two nearest neighbors, here we focus on the third and fourth steps.

1. Entanglement among 4 atoms

Here we consider a system consisting of only four atoms

$$A_1, \quad B_1, \quad C_1, \quad D_1,$$

as an example. The pumping for step 1 and 2 follow as

$$A_1, \quad B_1 \xrightarrow{\text{Step 1: pairwise entanglement}} |g_+\rangle,$$
$$C_1, \quad D_1 \xrightarrow{\text{Step 2: pairwise entanglement}} |g_+\rangle,$$

while step 3 is

$$B_1, \quad C_1 \xrightarrow{\text{Step 3: SWAP-gate}} B_1, \quad C_1 \text{ become entangled.}$$

Here pulse $1, 2, 3$ and $4, 5, 6$ are exactly the same as the three pulses in the main text. To illustrate the physics in step 3, we first write out the state after step 2 (here we assume perfect creation of ground Bell state for step 1 and 2),

$$\frac{1}{2}\left(|\uparrow\downarrow\rangle + |\downarrow\uparrow\rangle\right)_{A_1,B_1} \otimes \left(|\uparrow\downarrow\rangle + |\downarrow\uparrow\rangle\right)_{C_1,D_1},$$

then the two π pulses and 2π pulse of step 3 have the effect

$$
\begin{aligned}
&\text{Two two-photon Rabi processes via 5P, 6P states of atom } C_1, \quad T_1 = \frac{\pi}{\Omega}, \text{reaching n = 73 Rydberg state} \\
\xrightarrow{\text{pulse 7}} \quad & \frac{1}{2}\left(|\uparrow\downarrow\rangle + |\downarrow\uparrow\rangle\right)_{A_1,B_1} \otimes \left(|\Downarrow\downarrow\rangle + |\Uparrow\uparrow\rangle\right)_{C_1,D_1} = \frac{1}{2}\left(|\uparrow\downarrow\Uparrow\uparrow\rangle + |\downarrow\uparrow\Downarrow\downarrow\rangle + |\uparrow\downarrow\Downarrow\downarrow\rangle + |\downarrow\uparrow\Uparrow\uparrow\rangle\right)_{A_1,B_1,C_1,D_1}, \\
&\text{Two two-photon Rabi processes via 5P, 6P states of atom } B_1, \quad T_2 \approx \frac{2\pi}{\Omega}, \text{using n = 75 Rydberg state} \\
\xrightarrow{\text{pulse 8}} \quad & \frac{1}{2}\left(|\uparrow\downarrow\Uparrow\uparrow\rangle + |\downarrow\uparrow\Downarrow\downarrow\rangle - |\uparrow\uparrow\Uparrow\downarrow\rangle - |\downarrow\downarrow\Downarrow\uparrow\rangle\right)_{A_1,B_1,C_1,D_1}, \\
&\text{Two two-photon Rabi processes via 5P, 6P states of atom } C_1, \quad T_3 = \frac{\pi}{\Omega}, \text{depopulating n = 73 Rydberg state} \\
\xrightarrow{\text{pulse 9}} \quad & \frac{1}{2}\left(|\uparrow\downarrow\downarrow\uparrow\rangle + |\downarrow\uparrow\uparrow\downarrow\rangle - |\uparrow\uparrow\downarrow\downarrow\rangle - |\downarrow\downarrow\uparrow\uparrow\rangle\right)_{A_1,B_1,C_1,D_1}. \qquad \text{(E3)}
\end{aligned}
$$

where we assume that the state $|\downarrow\Uparrow\rangle_{B_1,C_1}$ can not be excited to state $|\Uparrow\Uparrow\rangle_{B_1,C_1}$ (similar for the other state $|\uparrow\Downarrow\rangle_{B_1,C_1}$) during pulse 8, simply because (the value is for two nearest-neighboring atoms)

$$V_1^{(73,75)}(1,1)/(2\pi) = V_1^{(73,75)}(4,4)/(2\pi) \approx 0.5\text{MHz},$$

is much larger than any other rates in the model. Here we have labeled the two Rabi frequencies $\Omega_{\rm A}, \Omega^{\rm A}$ during pulse 7 and 9, and $\Omega_{\rm B}, \Omega^{\rm B}$ during pulse 8 as Ω. Pulse 7 and 9 are simply π pulses. To understand the 2π pulse (i.e., pulse 8) above, let us write the Hamiltonian

$$\hat{H}^{(1)}_{\text{Pulse 8}} = \frac{1}{2\sqrt{2}} \begin{pmatrix} 0 & 0 & \Omega e^{i\phi} & -\Omega e^{i\phi} \\ 0 & 0 & \Omega e^{i\phi} & \Omega e^{i\phi} \\ \Omega e^{-i\phi} & \Omega e^{-i\phi} & 2\sqrt{2}V_+ & 0 \\ -\Omega e^{-i\phi} & \Omega e^{-i\phi} & 0 & 2\sqrt{2}V_- \end{pmatrix}, \qquad \text{(E4)}$$

where the basis vectors are $|\uparrow\Uparrow\rangle_{B_1,C_1}$, $|\downarrow\Downarrow\rangle_{B_1,C_1}$, $|r_+\rangle_{B_1,C_1}$ and $|r_-\rangle_{B_1,C_1}$, and ϕ is similar to $\phi_{\rm B} = \phi^{\rm B}$ in the main text. To have an analytical result, we neglect the population on $|r_-\rangle_{B_1,C_1}$, and also approximate $V_+ \approx 0$, then we have

$$
\begin{aligned}
|\downarrow\Downarrow\rangle &\xrightarrow{2\pi \text{ pulse with Rabi frequency } \Omega} -|\uparrow\Uparrow\rangle, \\
|\uparrow\Uparrow\rangle &\xrightarrow{2\pi \text{ pulse with Rabi frequency } \Omega} -|\downarrow\Downarrow\rangle. \qquad \text{(E5)}
\end{aligned}
$$

From Eq. (E3), it is clear that in the computation basis $|\uparrow\uparrow\rangle$, $|\uparrow\downarrow\rangle$, $|\downarrow\uparrow\rangle$, $|\downarrow\downarrow\rangle$, we have simply realized a SWAP-like gate that can be represented by the matrix (taking into account the π-phase on each basis state due to optical excitation of pulse 7 and 9 on atom C_1)

$$\overline{\text{SWAP}} = \begin{pmatrix} -1 & 0 & 0 & 0 \\ 0 & 0 & 1 & 0 \\ 0 & 1 & 0 & 0 \\ 0 & 0 & 0 & -1 \end{pmatrix}, \qquad \text{(E6)}$$

which is very similar to a SWAP gate, up to a π phase change on the basis states $|\uparrow\downarrow\rangle$, $|\downarrow\uparrow\rangle$ relative to the basis states $|\uparrow\uparrow\rangle$, $|\downarrow\downarrow\rangle$.

Here, the Rabi frequencies in pulse 7 and pulse 9 are only limited by the available laser, since there is one (approximately one) Rydberg excitation during pulse 7 (9). However, we shall use typical Rabi frequency $\sqrt{V_+V_-}$ during pulse 8. By choosing $\Omega = 89$kHz and pulse duration $t_{pulse8} = 11.12\mu s$, we numerically solve the state evolution by Eq. (E4) and find that pulse 8 can transform from state $|\uparrow\Uparrow\rangle$ to state $|\downarrow\Downarrow\rangle_{B_1,C_1}$ with a fidelity $\mathcal{F}_{\downarrow\uparrow} = 96.649\%$ (the remaining population is mainly in $|\downarrow\Downarrow\rangle$), as shown in Fig. 8. Following pulse 8, pulse 9 shall be a π pulse transferring $|\downarrow\Downarrow\rangle_{B_1,C_1}$ back to $|\uparrow\downarrow\rangle$, although pulse 9 will also transfer $\sim \sqrt{0.033}|\downarrow\Downarrow\rangle$ back to and up from $|\downarrow\uparrow\rangle$. Neglecting population on $|\downarrow\Downarrow\rangle_{B_1,C_1}$, then pulses 7,8 and 9 have the following property,

$$
\begin{aligned}
|\downarrow\uparrow\rangle &\xrightarrow[\text{atom}C_1]{\pi} -i|\downarrow\Downarrow\rangle \xrightarrow[\text{atom}B_1]{2\pi} i|\uparrow\Uparrow\rangle \xrightarrow[\text{atom}C_1]{\pi} |\uparrow\downarrow\rangle, \\
|\uparrow\downarrow\rangle &\xrightarrow[\text{atom}C_1]{\pi} -i|\uparrow\Uparrow\rangle \xrightarrow[\text{atom}B_1]{2\pi} i|\downarrow\Downarrow\rangle \xrightarrow[\text{atom}C_1]{\pi} |\downarrow\uparrow\rangle,
\end{aligned}
$$

where pulse 7 and 9 can be ideal π pulses. To find the fidelity of the gate through pulse 7 to pulse 9, we shall also study state evolution of $|\uparrow\uparrow\rangle$, $|\downarrow\downarrow\rangle$. Choosing initial state $|\uparrow\uparrow\rangle$, then pulse 8 have the Hamiltonian beginning with state $-i|\uparrow\Downarrow\rangle$

$$\hat{H}^{(2)}_{\text{Pulse 8}} = \begin{pmatrix} 0 & \frac{1}{2}\Omega e^{i\phi(B_1)} \\ \frac{1}{2}\Omega e^{i\phi(B_1)} & V_{73,75}(4,4) \end{pmatrix}, \qquad \text{(E7)}$$

which gives us a population of $\mathcal{F}_{\uparrow\uparrow} = 99.976\%$ on state $|\uparrow\Downarrow\rangle$ at the end of pulse 8 with $\Omega = 89$kHz. Note that pulse 9 can ideally transfer this state back to $|\uparrow\uparrow\rangle$ in MHz rate. Then the fidelity of the SWAP-like gate is

$$\mathcal{F}_{\text{SWAP}} \equiv \frac{1}{4}(\mathcal{F}_{\uparrow\downarrow} + \mathcal{F}_{\downarrow\uparrow} + \mathcal{F}_{\uparrow\uparrow} + \mathcal{F}_{\downarrow\downarrow}) = 98.31\%. \qquad \text{(E8)}$$

2. Entanglement among 6 atoms

A minimal model to illustrate global entanglement of $4N$ atoms can be shown by a system consisting of only

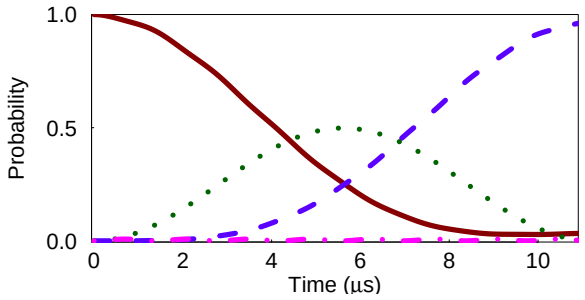

FIG. 8: (Color online) State evolution starting from $|\uparrow\Uparrow\rangle$. The (red) solid, (blue) dashed, (green) dotted, and (magenta) dash-dotted curves represent population on state $|\uparrow\Uparrow\rangle_{B_1,C_1}$, $|\downarrow\Downarrow\rangle_{B_1,C_1}$, $|r_+\rangle_{B_1,C_1}$ and $|r_-\rangle_{B_1,C_1}$, respectively. Here $\Omega = 89$kHz. At the end of pulse duration $t_{pulse8} = 11.12\mu s$ (this duration is $0.12\mu s$ shorter than $2\pi/\Omega$), $|\langle\Psi|\ \downarrow\Downarrow\rangle_{B_1,C_1}|^2 = 96.649\%$.

six atoms. In order to characterize the entanglement, we consider a system consisting of the following six atoms

$$A_1,\quad B_1,\quad C_1,\quad D_1,\quad A_2,\quad B_2, \tag{E9}$$

as an example. The pumping for step 1 and 2 follows as

$$\begin{aligned} A_1,\ B_1;\ A_2,\ B_2 &\xrightarrow{\text{Step 1: pairwise entanglement}} |g_+\rangle\otimes|g_+\rangle,\\ C_1,\ D_1 &\xrightarrow{\text{Step 2: pairwise entanglement}} |g_+\rangle, \end{aligned}$$

while step 3 and step 4 are

$$\begin{aligned} B_1,\ C_1 &\xrightarrow{\text{Step 3: SWAP-gate}} B_1,\ C_1 \text{ become entangled},\\ D_1,\ A_2 &\xrightarrow{\text{Step 4: SWAP-gate}} D_1,\ A_2 \text{ become entangled}. \end{aligned}$$

After step 3, we have a state in Eq. (E3) for A_1, B_1, C_1, D_1. To illustrate the physics in step 4, we first write out the state after step 3 (here we assume perfect creation of ground Bell state for step 1 and 2, and entanglement in step 3),

$$\frac{1}{2\sqrt{2}}\left(|\uparrow\downarrow\downarrow\uparrow\rangle + |\downarrow\uparrow\uparrow\downarrow\rangle - |\uparrow\uparrow\downarrow\downarrow\rangle - |\downarrow\downarrow\uparrow\uparrow\rangle\right)_{A_1,B_1,C_1,D_1} \otimes \left(|\uparrow\downarrow\rangle + |\downarrow\uparrow\rangle\right)_{A_2,B_2}.$$

The pulse in this final step is exactly the same as in Eq. (E3).

Two two-photon Rabi processes via 5P, 6P states of atom A_2, $T_1 = \dfrac{\pi}{\Omega}$, reaching n = 73 Rydberg state

$$\xrightarrow{\text{pulse 10}} \frac{1}{2\sqrt{2}}\left[(|\uparrow\downarrow\downarrow\rangle - |\downarrow\downarrow\uparrow\rangle)\,|\uparrow\rangle + (|\downarrow\uparrow\uparrow\rangle - |\uparrow\uparrow\downarrow\rangle)\,|\downarrow\rangle\right]_{A_1,B_1,C_1,D_1} \otimes \left(|\Downarrow\downarrow\rangle + |\Uparrow\uparrow\rangle\right)_{A_2,B_2}$$
$$= \frac{1}{2\sqrt{2}}\left[(|\uparrow\downarrow\downarrow\rangle - |\downarrow\downarrow\uparrow\rangle)\,|\uparrow\Downarrow\downarrow\rangle + (|\downarrow\uparrow\uparrow\rangle - |\uparrow\uparrow\downarrow\rangle)\,|\downarrow\Downarrow\downarrow\rangle + (|\uparrow\downarrow\downarrow\rangle - |\downarrow\downarrow\uparrow\rangle)\,|\uparrow\Uparrow\uparrow\rangle + (|\downarrow\uparrow\uparrow\rangle - |\uparrow\uparrow\downarrow\rangle)\,|\downarrow\Uparrow\uparrow\rangle\right],$$

Two two-photon Rabi processes via 5P, 6P states of atom D_1, $T_2 \approx \dfrac{2\pi}{\Omega}$, using n = 75 Rydberg state

$$\xrightarrow{\text{pulse 11}} \frac{1}{2\sqrt{2}}\left[(|\uparrow\downarrow\downarrow\rangle - |\downarrow\downarrow\uparrow\rangle)\,|\uparrow\Downarrow\downarrow\rangle - (|\downarrow\uparrow\uparrow\rangle - |\uparrow\uparrow\downarrow\rangle)\,|\uparrow\Uparrow\downarrow\rangle - (|\uparrow\downarrow\downarrow\rangle - |\downarrow\downarrow\uparrow\rangle)\,|\downarrow\Downarrow\uparrow\rangle + (|\downarrow\uparrow\uparrow\rangle - |\uparrow\uparrow\downarrow\rangle)\,|\downarrow\Uparrow\uparrow\rangle\right],$$

Two two-photon Rabi processes via 5P, 6P states of atom A_2, $T_3 = \dfrac{\pi}{\Omega}$, depopulating n = 73 Rydberg state

$$\xrightarrow{\text{pulse 12}} \frac{1}{2\sqrt{2}}\left[(|\uparrow\downarrow\downarrow\rangle - |\downarrow\downarrow\uparrow\rangle)\,|\uparrow\uparrow\downarrow\rangle - (|\downarrow\uparrow\uparrow\rangle - |\uparrow\uparrow\downarrow\rangle)\,|\uparrow\downarrow\downarrow\rangle - (|\uparrow\downarrow\downarrow\rangle - |\downarrow\downarrow\uparrow\rangle)\,|\downarrow\uparrow\uparrow\rangle + (|\downarrow\uparrow\uparrow\rangle - |\uparrow\uparrow\downarrow\rangle)\,|\downarrow\downarrow\uparrow\rangle\right]$$
$$= \frac{1}{2\sqrt{2}}\left[(|\uparrow\downarrow\downarrow\rangle - |\downarrow\downarrow\uparrow\rangle)_{A_1,B_1,C_1}\,(|\uparrow\uparrow\downarrow\rangle - |\downarrow\uparrow\uparrow\rangle)_{D_1,A_2,B_2} + (|\downarrow\uparrow\uparrow\rangle - |\uparrow\uparrow\downarrow\rangle)_{A_1,B_1,C_1}\,(|\downarrow\downarrow\uparrow\rangle - |\uparrow\downarrow\downarrow\rangle)_{D_1,A_2,B_2}\right].$$

[1] A. Einstein, B. Podolsky, and N. Rosen, Phys. Rev. **47**, 777 (1935).

[2] M. A. Nielsen and I. L. Chuang, *Quantum Computation and Quantum Information* (Cambridge University Press, Cambridge, 2000).

[3] C. Adams and E. Riis, Progress in Quantum Electronics

21, 1 (1997).
[4] D. Møller, L. B. Madsen, and K. Mølmer, Phys. Rev. Lett. **100**, 170504 (2008).
[5] M. Saffman and K. Mølmer, Phys. Rev. Lett. **102**, 240502 (2009).
[6] B. Zhao, M. Müller, K. Hammerer, and P. Zoller, Phys. Rev. A **81**, 052329 (2010).
[7] M. Saffman, T. G. Walker, and K. Mølmer, Rev. Mod. Phys. **82**, 2313 (2010).
[8] L. Isenhower, E. Urban, X. L. Zhang, A. T. Gill, T. Henage, T. A. Johnson, T. G. Walker, and M. Saffman, Phys. Rev. Lett. **104**, 010503 (2010).
[9] E. Urban, T. A. Johnson, T. Henage, L. Isenhower, D. D. Yavuz, T. G. Walker, and M. Saffman, Nature Phys. **5**, 110 (2009).
[10] X. L. Zhang, A. T. Gill, L. Isenhower, T. G. Walker, and M. Saffman, Phys. Rev. A **85**, 042310 (2012).
[11] A. W. Carr and M. Saffman, Phys. Rev. Lett. **111**, 033607 (2013).
[12] D. D. Bhaktavatsala Rao and K. Mø lmer, Phys. Rev. Lett. **111**, 033606 (2013).
[13] D. Tong, S. M. Farooqi, J. Stanojevic, S. Krishnan, Y. P. Zhang, R. Côté, E. E. Eyler, and P. L. Gould, Phys. Rev. Lett. **93**, 063001 (2004).
[14] R. Heidemann, U. Raitzsch, V. Bendkowsky, B. Butscher, R. Löw, L. Santos, and T. Pfau, Phys. Rev. Lett. **99**, 163601 (2007).
[15] T. Vogt, M. Viteau, A. Chotia, J. Zhao, D. Comparat, and P. Pillet, Phys. Rev. Lett. **99**, 073002 (2007).
[16] A. Schwarzkopf, R. E. Sapiro, and G. Raithel, Phys. Rev. Lett. **107**, 103001 (2011).
[17] Y. O. Dudin and A. Kuzmich, Science **336**, 887 (2012).
[18] Y. O. Dudin, L. Li, F. Bariani, and A. Kuzmich, Nature Phys. **8**, 790 (2012).
[19] M. Viteau, P. Huillery, M. G. Bason, N. Malossi, D. Ciampini, O. Morsch, E. Arimondo, D. Comparat, and P. Pillet, Phys. Rev. Lett. **109**, 053002 (2012).
[20] D. Barredo, S. Ravets, H. Labuhn, L. Béguin, A. Vernier, F. Nogrette, T. Lahaye, and A. Browaeys, Phys. Rev. Lett. **112**, 183002 (2014).
[21] C. S. E. van Ditzhuijzen, A. F. Koenderink, J. V. Hernández, F. Robicheaux, L. D. Noordam, and H. B. V. L. van den Heuvell, Phys. Rev. Lett. **100**, 243201 (2008).
[22] J. Han and T. Gallagher, Phys. Rev. A **79**, 053409 (2009).
[23] F. Bariani, Y. O. Dudin, T. A. B. Kennedy, and A. Kuzmich, Phys. Rev. Lett. **108**, 030501 (2012).
[24] G. Günter, H. Schempp, M. Robert-de Saint-Vincent, V. Gavryusev, S. Helmrich, C. S. Hofmann, S. Whitlock, and M. Weidemüller, Science (New York, N.Y.) **342**, 954 (2013).
[25] H. Gorniaczyk, C. Tresp, J. Schmidt, H. Fedder, and S. Hofferberth, Phys. Rev. Lett. **113**, 053601 (2014).
[26] D. Tiarks, S. Baur, K. Schneider, S. Dürr, and G. Rempe, Phys. Rev. Lett. **113**, 053602 (2014).
[27] W. Li, D. Viscor, S. Hofferberth, and I. Lesanovsky, Phys. Rev. Lett. **112**, 243601 (2014).
[28] D. Paredes-Barato and C. S. Adams, Phys. Rev. Lett. **112**, 040501 (2014).
[29] T. G. Walker and M. Saffman, Phys. Rev. A **77**, 032723 (2008).
[30] W. Li, I. Mourachko, M. W. Noel, and T. F. Gallagher, Phys. Rev. A **67**, 052502 (2003).
[31] B. Kaulakys, J. Phys. B **28**, 4963 (1995).
[32] S.-Y. Lan, A. G. Radnaev, O. A. Collins, D. N. Matsukevich, T. A. Kennedy, and A. Kuzmich, Opt. Express **17**, 13639 (2009).
[33] M. E. Rose, *Elementary theory of angular momentum* (John Wiley & Sons, Inc., New York, 1957).
[34] S. D. Jenkins, Y. O. Dudin, R. Zhao, D. N. Matsukevich, A. Kuzmich, and T. A. B. Kennedy, J. Phys. B **45**, 124006 (2012).
[35] D. F. V. James, Fortschr. Phys. **48**, 823 (2000).
[36] E. Brion, L. H. Pedersen, and K. Mø lmer, J. Phys. A: Math. Theor. **40**, 1033 (2007).
[37] R. Han, H. K. Ng, and B.-G. Englert, J. Mod. Opt. **60**, 255 (2013).